

Thermal Boundary Resistance of W/Al₂O₃ Interface in W/Al₂O₃/W Three-Layered Thin Film and Its Dependence on Morphology

Shizuka Kawasaki¹, Yuichiro Yamashita^{2*}, Nobuto Oka¹, Takashi Yagi², Junjun Jia¹, Naoyuki Taketoshi², Tetsuya Baba², and Yuzo Shigesato¹

¹Graduate School of Science and Engineering, Aoyama Gakuin University, Sagamihara 252-5258, Japan

²National Metrology Institute of Japan (NMIJ), National Institute of Advanced Industrial Science and Technology (AIST), Tsukuba, Ibaraki 305-8563, Japan

E-mail: yuichiro-yamashita@aist.go.jp

Received February 6, 2013; accepted March 28, 2013; published online May 24, 2013

We investigated the dependence of the thermal boundary resistance of the W/Al₂O₃ interface in W/Al₂O₃/W three-layered thin films on the interface morphology. The layered structures, Al₂O₃ thin layers with thicknesses from 1 to 50 nm covered by top and bottom W layers with a thickness of 100 nm, were fabricated by magnetron sputtering using a W target (99.99%) and an Al₂O₃ target (99.99%). The fabrication of polycrystalline W and amorphous Al₂O₃ films was confirmed by structural analysis. The morphology of the bottom W layer/Al₂O₃ layer and Al₂O₃ layer/top W layer interfaces showed a wavelike structure with a roughness of about 1 nm. Thermophysical properties and thermal boundary resistance were measured by a pulsed light heating thermoreflectance technique. The thermal boundary resistance of the W/Al₂O₃ interface was $1.9 \times 10^{-9} \text{ m}^2 \text{ K W}^{-1}$, which corresponds to the thermal resistance of a 3.7-nm-thick Al₂O₃ film or a 120-nm-thick W film.

© 2013 The Japan Society of Applied Physics

1. Introduction

The thermal boundary resistance (TBR), number of interfaces per unit length, and thermal conductivity of each layer are important factors for determining the overall thermal resistance of a multilayered thin film. The most important factor is the carrier that dominates the heat conduction of the layers of both sides of the interface. Heat is mainly carried by electrons in pure metals, whereas it is carried by phonons in dense insulators. Therefore, there is an essential difference in the mechanism of TBR of metal/metal,^{1,2)} metal/insulator,^{3,4)} and insulator/insulator interfaces. Since both electrons and phonons contribute to heat conduction in semiconductors and electrical conducting transparent thin films,⁵⁻⁹⁾ the mechanism is even more complex when both or either side of the interface is semiconductor or an electrical conducting transparent thin film. It is also proposed that TBR is related to phonon mismatch at the interface formed by dissimilar substances.

In the case of the W/Al₂O₃ interface, electrons are the main heat carriers in tungsten and only phonons are the heat carriers in alumina. Thus, the TBR between one thin film where electrons are the main heat carriers and another thin film where only phonons are the heat carriers is discussed in this study.

There are also many factors that affect on thermal resistance in the interface region disordered by chemical reaction,^{10,11)} contamination, or roughness,¹²⁾ these are assigned to a scale larger than the atomic level. The thermal resistances originated in these larger-scale effects are reported to be as large as the order of 1×10^{-8} to $1 \times 10^{-5} \text{ m}^2 \text{ K W}^{-1}$; however, these larger-scale effects are outside the scope of this study. According to the measurements obtained by pulsed light heating thermoreflectance methods under the configuration of rear heating and front temperature detection, which is also called the ultrafast laser flash method,¹³⁻¹⁵⁾ the TBR of metal/oxide interfaces ranges from 1×10^{-9} to $1 \times 10^{-8} \text{ m}^2 \text{ K W}^{-1}$,^{3,4,16-19)} which is equivalent to the thermal resistance of several-ten-nm-thick oxide films, whereas the TBR of metal/metal interfaces ranges from 1×10^{-10} to $1 \times 10^{-9} \text{ m}^2 \text{ K W}^{-1}$.^{1,2)} In multilayered thin films, the maximum number of interfaces per unit length that can be

fabricated mainly depends on the morphology of the surface of the constituent layers. The thermal insulating performance resulting from the high-density package of interfaces in multilayered thin films was reported. Costescu et al.²⁰⁾ calculated the effective thermal conductivity to be $0.6 \text{ W m}^{-1} \text{ K}^{-1}$ for a few-nanometer-thick region of thin films including a W/Al₂O₃ interface, which is lower than the thermal conductivity of amorphous Al₂O₃, when the number of interfaces per unit length reached 0.4 nm^{-1} . This calculation suggests a reasonable conclusion, that is, high-density package of interfaces with ordered layer structures is necessary for realizing a higher thermal resistance in multilayered thin films. Oka et al.¹⁹⁾ observed heat transport across the Mo/Al₂O₃/Mo three-layered films after being heated by ultra-short laser pulses, where the thickness of the Al₂O₃ layer was varied from 0.5 to 100 nm. They obtained a TBR of $1.5 \times 10^{-9} \text{ m}^2 \text{ K W}^{-1}$ between the Al₂O₃ and Mo layers.

In both previous studies, the total thermal resistance of those metal/oxide three-layered thin films with oxide layers of several nanometers is smaller than the extrapolated values from the results of those with oxide layers thicker than 10 nm. They pointed out the possibilities that such thin Al₂O₃ layers could not perfectly separate metal layers and that both sides of metal layers could contact each other directly. However, the morphological characteristics of the film (e.g., surface roughness or nanoscale interfacial region) should be carefully observed and studied before drawing conclusions.

The purpose of this study is to understand the effect of nanoscale morphology on TBR. Firstly, we fabricated W/Al₂O₃/W three-layered thin films by paying careful attention to the reduction in the roughness of the interface. Secondly, we investigated the correlation between material characteristics and TBR systematically by quantitative thermophysical property measurement and structural analysis.

2. Experimental Methods

2.1 Sample preparation

To investigate the TBR of the Al₂O₃/W interface, a set of W/Al₂O₃/W three-layered films were prepared, as shown in Fig. 1(a). There are two interfaces in a three-layered

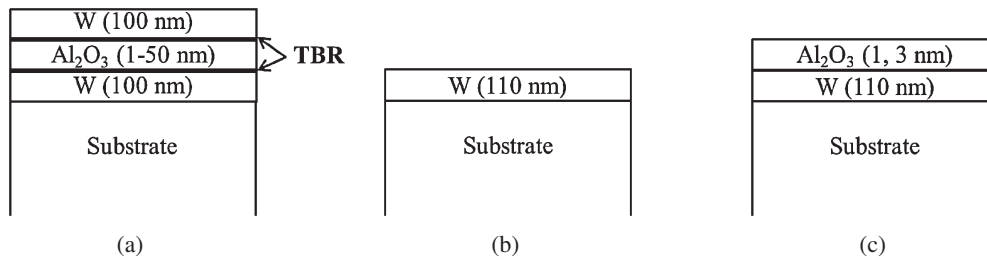


Fig. 1. Series of samples prepared for measurement of (a) thermal boundary resistance of W/Al₂O₃ interface, (b) morphology of bottom W layer, and (c) morphology of Al₂O₃ layer.

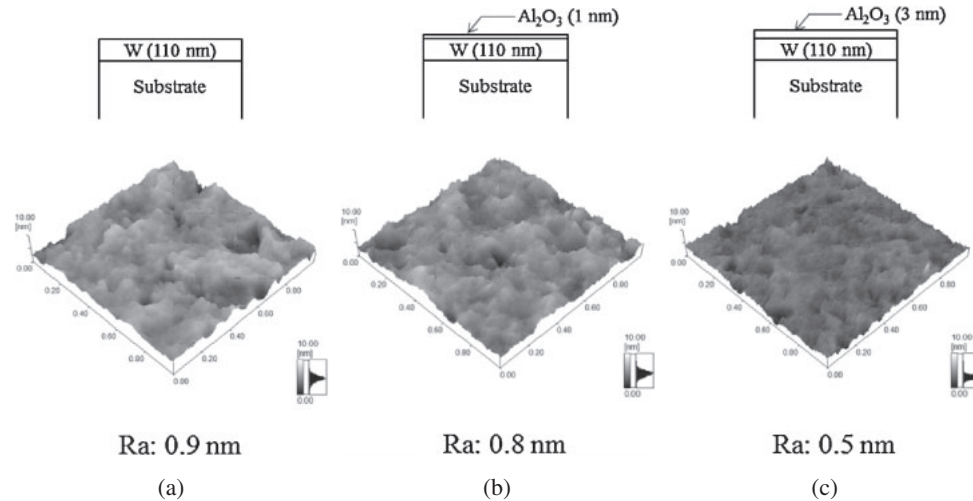


Fig. 2. Surface morphologies of (a) W film (110 nm), (b) Al₂O₃ (1 nm)/W (110 nm) film, and (c) Al₂O₃ (3 nm)/W (110 nm) film.

film. The Al₂O₃ layer thickness ($d_{\text{Al}_2\text{O}_3}$) was varied from 1 to 50 nm. In addition, a W monolayer film with a thickness of 210 nm was prepared as $d_{\text{Al}_2\text{O}_3} = 0$ nm sample.

Before sputtering, the sputtering chamber was evacuated to less than 7.0×10^{-4} Pa. Firstly, a bottom W layer (W_b) with a thickness of 100 nm was deposited on an alkali-free glass substrate by dc magnetron sputtering using a W target (99.99%, 3 in. in diameter) and a pure Ar gas ($\geq 99.999\%$) at a substrate temperature of 450 K. The sputtering was carried out at a total gas pressure of 1.0 Pa and a dc power of 100 W. Secondly, an Al₂O₃ layer was deposited on the bottom W layer by rf magnetron sputtering using an Al₂O₃ target (99.99%, 3 in. in diameter) and a pure Ar gas at 450 K. Here, the total gas pressure was 0.5 Pa and the rf power was 100 W. Finally, a top W layer (W_t) with a thickness of 100 nm was deposited on the Al₂O₃ layer again. The sputtering conditions of the top W layer were the same as those previously mentioned. Those W/Al₂O₃/W three-layered films were fabricated with no exposure to atmosphere between deposition processes.

In addition to the above samples, some monolayer and two-layer samples, as shown in Figs. 1(b) and 1(c), were prepared to observe their surface morphology and determine their phases (and other physical properties). Here, the sputtering conditions of those monolayer and two-layer films were the same as those of the three-layered films. The surface roughness was measured by atomic force microscopy (AFM; Shimadzu SPM-9500). The crystal structure was estimated by X-ray diffraction (XRD; Shimadzu XRD-6000).

2.2 Measurement of thermal boundary resistance of W/Al₂O₃ interface

A picosecond pulsed light heating thermoreflectance system^{13–15} was used to measure the TBR and thermal diffusivity. This system²¹ operates under the following principles to observe heat transfer across the thin film. A pump laser pulse with a wavelength of 1550 nm, a pulse width of 0.5 ps, and an optical power of 20 mW is focused on the rear side (transparent substrate side) of the W/Al₂O₃/W sample and a fraction of its energy is absorbed at the skin depth of the W layer and converted into heat. The generated heat diffuses one-dimensionally toward the front side of the sample when the laser spot size is much larger than the film thickness. A probe laser pulse with a wavelength of 775 nm, a pulse width of 0.5 ps, and an optical power of 1–2 mW is used to detect the temperature change at the front side as a change in reflectivity. The transient temperature is recorded as a function of the delay time relative to the pump laser pulse. To determine the thermal diffusivity of the Al₂O₃ film and the thermal boundary resistance between the Al₂O₃ and W films, a set of transient temperature data with different Al₂O₃ film thicknesses are analyzed by the areal heat diffusion time method.²²

3. Results and Discussion

3.1 Interface morphology and layered structure

The interface morphology and layered structure of the three-layered film were estimated using the separately fabricated W

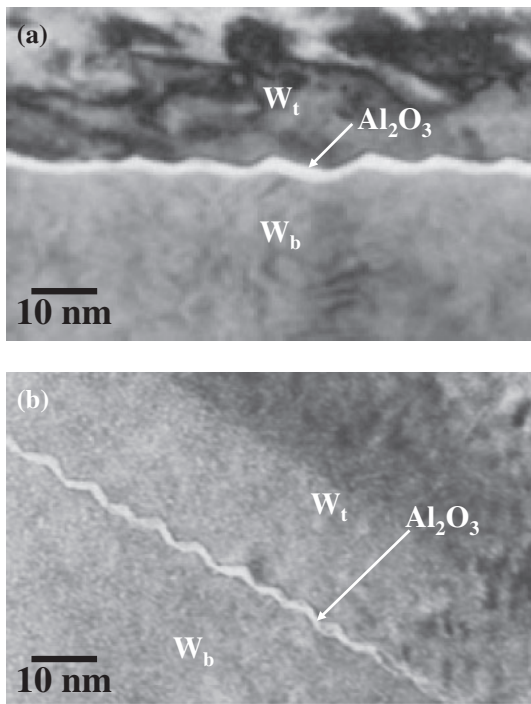


Fig. 3. Cross-sectional TEM images of W/Al₂O₃/W three-layered films with Al₂O₃ thicknesses of (a) 2 and (b) 1 nm.

monolayer and Al₂O₃/W two-layered films. Figure 2 shows the surface morphologies of the 110-nm-thick W monolayer film, 1-nm-thick Al₂O₃/110-nm-thick W film, and 3-nm-thick Al₂O₃/110-nm-thick W film measured by AFM. These morphologies can be the same as those of Al₂O₃/W_b and W_t/Al₂O₃ (1, 3 nm) interfaces in the three-layered films.

For the W monolayer film, the roughness (*R_a*) is 0.9 nm, which is attributed to the crystal growth of tungsten grains. The morphology of the Al₂O₃/W_b interface can be the same as the *R_a*. After the deposition of the 1-nm-thick Al₂O₃ film on the W monolayer film, *R_a* becomes 0.8 nm, as shown in Fig. 2(b). This roughness is almost comparable to the thickness of the Al₂O₃ film. As a result, it is controversial whether the 1-nm-thick Al₂O₃ layer can entirely cover the bottom W layer. If the 1-nm-thick Al₂O₃ layer does not isolate both metal layers in the three-layered films, part of the bottom W layer can contact directly with the top W layer. For the Al₂O₃ (3 nm)/W (110 nm) film, *R_a* decreases to 0.5 nm. Since this roughness is much smaller than the thickness of the Al₂O₃ layer, it can be considered that the 3-nm-thick Al₂O₃ layer is capable of isolating the metal layers in the three-layered film. Figure 3 shows the cross-sectional images of the three-layered films with *d*_{Al₂O₃} = 1 and 2 nm observed by transmission electron microscopy (TEM; JEOL JEM-4010). The Al₂O₃ layers are not straight but have fine curved interfaces along with the roughness of the W_b layer. The amplitude of the wave is about 1.5 nm, which agrees with *R_a* (0.9 nm) observed by AFM. The thickness of Al₂O₃ layer is comparable to the roughness of the interface, as shown in the AFM results. The layered structure of the 1-nm-thick Al₂O₃ layer is partially not distinct and there is a possibility for the existence of contact regions between the W_b and W_t layers. On the other hand, the 2-nm-thick Al₂O₃ layer seems to isolate the W layers.

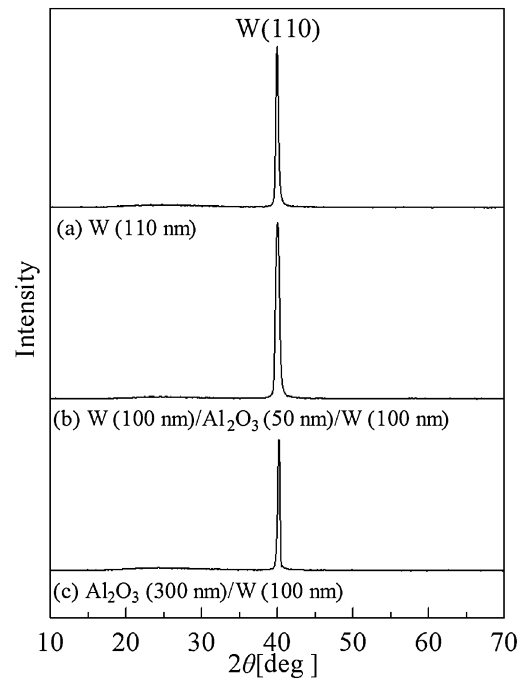


Fig. 4. XRD patterns of (a) W (110 nm), (b) W (100 nm)/Al₂O₃ (50 nm)/W (100 nm), and (c) Al₂O₃ (300 nm)/W (100 nm) films.

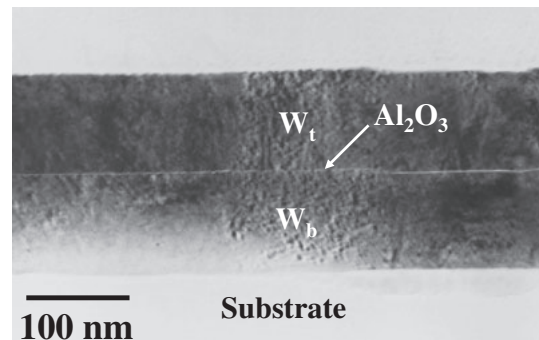


Fig. 5. Cross-sectional TEM image of W/Al₂O₃/W three-layered films with Al₂O₃ layer of 1 nm thickness.

Figure 4 shows the XRD results of some layered samples. For the 110-nm-thick W monolayer film, the diffraction peak from the W(110) plane was observed at 40.3°. From this XRD result, the W_b layer was considered the polycrystalline and its estimated grain size was 24 nm. The XRD pattern of the W/Al₂O₃ (50 nm)/W three-layered film only shows a peak from the W(110) plane at 40.3°. On the basis of these data, there is no difference between the W_b and W_t layers. On the other hand, no Al₂O₃ peaks were observed. We also prepared an Al₂O₃ (300 nm)/W (110 nm) two-layered film for XRD measurement as shown in Fig. 4(c), but still no peaks from Al₂O₃ planes were observed. Thus, it can be considered that the Al₂O₃ layers in the W/Al₂O₃/W three-layered film were amorphous.

3.2 Analysis of transient temperature of W/Al₂O₃/W three-layered films and thermal boundary resistance of W/Al₂O₃ interface

Figure 5 shows a cross-sectional TEM image of the W/Al₂O₃/W three-layered thin film with an Al₂O₃ layer of

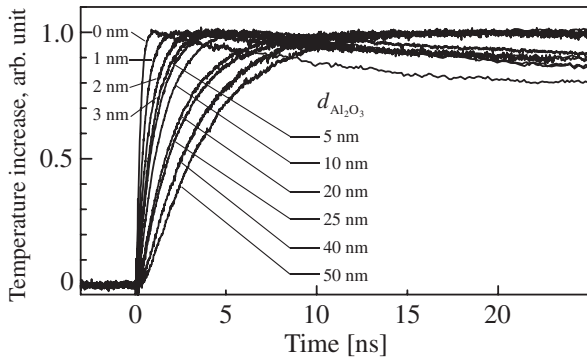


Fig. 6. Transient temperatures of W (100 nm)/Al₂O₃/W (100 nm) three-layered films with Al₂O₃ layers of thicknesses ($d_{\text{Al}_2\text{O}_3}$) from 0 to 50 nm. The $d_{\text{Al}_2\text{O}_3}$ values are shown in this figure. Here, the film of $d_{\text{Al}_2\text{O}_3} = 0$ nm is a W monolayer film with a thickness of 210 nm.

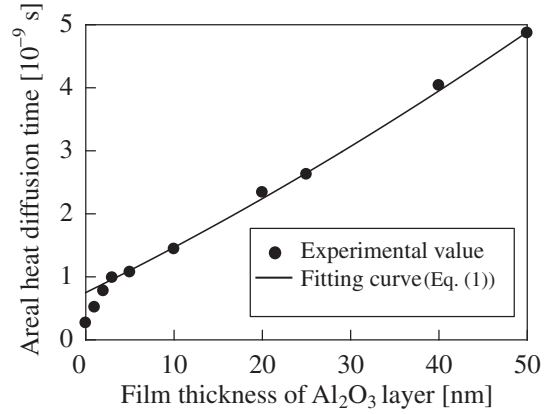


Fig. 7. Areal heat diffusion time of W/Al₂O₃/W three-layered films versus the Al₂O₃ layer thickness.

1 nm thickness. The three-layered structure was fabricated and the film thicknesses of the W_t and W_b layers were about 100 nm. Figure 6 shows the transient temperatures of the W/Al₂O₃/W three-layered films with Al₂O₃ layers with thicknesses from 0 to 50 nm. The rate of temperature increase decreases with increasing Al₂O₃ layer thickness.

The TBR between the W and Al₂O₃ layers was determined by the areal heat diffusion time method.²²⁾ From Fig. 6, the areal heat diffusion time is defined as the area surrounded by the transient temperature, a horizontal line at normalized temperature = 1 and $t = 0$, which can be described as^{22,23)}

$$A = \left(\frac{\left(C_{\text{Al}_2\text{O}_3} d_{\text{Al}_2\text{O}_3} + \frac{4}{3} C_W d_W \right) \frac{d_W^2}{\kappa_W} + \left(\frac{C_W^2 d_W^2}{C_{\text{Al}_2\text{O}_3} d_{\text{Al}_2\text{O}_3} + \frac{1}{6} C_{\text{Al}_2\text{O}_3} d_{\text{Al}_2\text{O}_3} + C_W d_W \right) \frac{d_{\text{Al}_2\text{O}_3}^2}{\kappa_{\text{Al}_2\text{O}_3}}}{C_{\text{Al}_2\text{O}_3} d_{\text{Al}_2\text{O}_3} + 2 C_W d_W} \right) + \frac{2 C_W d_W (C_{\text{Al}_2\text{O}_3} d_{\text{Al}_2\text{O}_3} + C_W d_W)}{C_{\text{Al}_2\text{O}_3} d_{\text{Al}_2\text{O}_3} + 2 C_W d_W} R_{\text{bd}}, \quad (1)$$

where A is the areal heat diffusion time, C is the heat capacity per unit volume, d is the film thickness, κ is the thermal diffusivity, and R_{bd} is the thermal boundary resistance. Here, the subscripts indicate the layers. Before the analysis, we measured the thermal diffusivity of the W monolayer (κ_W) as $2.5 \times 10^{-5} \text{ m}^2 \text{ s}^{-1}$. The heat capacity per unit volume of W (C_W) was $2.55 \times 10^6 \text{ J m}^{-3} \text{ K}^{-1}$, which was derived from the density of 19300 kg m^{-3} ²⁴⁾ and the specific heat capacity of $132 \text{ J kg}^{-1} \text{ K}^{-1}$.²⁴⁾ The specific heat capacity of the Al₂O₃ was $775 \text{ J kg}^{-1} \text{ K}^{-1}$.²⁴⁾ For the Al₂O₃ density, the Al₂O₃ monolayer film with a thickness of 190 nm was measured by an X-ray reflectivity technique (XRR; Rigaku SmartLab), and the value was 3080 kg m^{-3} . The heat capacity per unit volume of the Al₂O₃ ($C_{\text{Al}_2\text{O}_3}$) film was thereby derived to be $2.39 \times 10^6 \text{ J m}^{-3} \text{ K}^{-1}$.

Figure 7 shows the areal heat diffusion time of the W/Al₂O₃/W three-layered films as a function of Al₂O₃ interlayer thickness. The curve in this figure shows the fitting result of Eq. (1), where the data of $d_{\text{Al}_2\text{O}_3} = 0, 1,$ and 2 nm are excluded from the fitting. The R_{bd} between the Al₂O₃ and W films is $1.9 \times 10^{-9} \text{ m}^2 \text{ K W}^{-1}$, which corresponds to the thermal resistance of a 3.7-nm-thick Al₂O₃ film or a 120-nm-thick W film. Our TBR is about half of the value of $3.8 \times 10^{-9} \text{ m}^2 \text{ K W}^{-1}$ reported by Costescu et al.²⁰⁾ The observed thermal diffusivity of the Al₂O₃ layer is $8.1 \times 10^{-7} \text{ m}^2 \text{ s}^{-1}$, which is much lower than that of a sapphire crystal ($1.5 \times 10^{-5} \text{ m}^2 \text{ s}^{-1}$),²⁴⁾ but is almost the same as the value of

$9.5 \times 10^{-7} \text{ m}^2 \text{ s}^{-1}$ for the amorphous Al₂O₃ films reported by Oka et al.¹⁹⁾

In Fig. 7, it is noted that the areal heat diffusion times of the 1 and 2 nm Al₂O₃ interlayer decrease from the curve of Eq. (1). As previously mentioned, we suppose that the 1-nm-thick Al₂O₃ layer does not entirely cover the W_b layer from the AFM and TEM results. Therefore, the direct contacts between the W layers seem to lead to the decrease as observed by Oka et al.¹⁹⁾ The 2-nm-thick Al₂O₃ layer seems to isolate the W layers as observed by TEM, but the existence of direct contact cannot be excluded completely. Consequently, regardless of the formation of the Al₂O₃/W flat interface, the decrease in areal heat diffusion time occurs when the Al₂O₃ interlayer is thinner than 2 nm. In this study, the nature of this decrease cannot be concluded because the contributions of electron heat conduction on direct contact, quantum effects, and heat transport of thin interlayers are not clear.

4. Conclusions

The dependence of TBR of the Al₂O₃/W interface in the W/Al₂O₃/W three-layered thin film on the interface morphology was investigated. W/Al₂O₃/W three-layered thin films were fabricated by sputtering. The thermophysical properties of each constituent layer and TBR of Al₂O₃/W interface were evaluated using a pulsed light heating thermoreflectance system. Consequently, the TBR of the Al₂O₃/W interface was found to be $1.9 \times 10^{-9} \text{ m}^2 \text{ K W}^{-1}$, which corre-

sponds to the thermal resistance of a 3.7-nm-thick Al_2O_3 film or a 120-nm-thick W film. When the Al_2O_3 interlayer thickness was below 2 nm, the areal heat diffusion time decreased from the extrapolated values from the results of those with oxide layers thicker than 3 nm. The heat transport mechanism that leads to the decrease in areal heat diffusion time is under discussion. In future works, to determine the origin of the mechanism, two possible heat transport mechanisms will be investigated. One is electron heat conduction by direct contact between metal layers and the other is heat transport driven by quantum effects.

Acknowledgement

The authors would like to thank Dr. Katsuhiko Inaba and Mr. Takayuki Konya of Rigaku Corporation for film density analysis.

- 1) T. Baba and N. Taketoshi: 20th Japan Symp. Thermophysical Properties, 1999, B114 [in Japanese].
- 2) H. Aoyama, T. Yagi, N. Taketoshi, T. Baba, A. Miyamura, Y. Sato, and Y. Shigesato: 28th Japan Symp. Thermophysical Properties, 2007, C142 [in Japanese].
- 3) R. Arisawa, T. Yagi, N. Taketoshi, T. Baba, A. Miyamura, Y. Sato, and Y. Shigesato: 28th Japan Symp. Thermophysical Properties, 2007, C132 [in Japanese].
- 4) R. Arisawa, T. Yagi, N. Taketoshi, T. Baba, A. Miyamura, Y. Sato, and Y. Shigesato: 27th Japan Symp. Thermophysical Properties, 2006, X213 [in Japanese].
- 5) T. Ashida, A. Miyamura, Y. Sato, T. Yagi, N. Taketoshi, T. Baba, and Y. Shigesato: *J. Vac. Sci. Technol. A* **25** (2007) 1178.
- 6) T. Ashida, A. Miyamura, N. Oka, Y. Sato, T. Yagi, N. Taketoshi, T. Baba, and Y. Shigesato: *J. Appl. Phys.* **105** (2009) 073709.
- 7) N. Oka, K. Kimura, T. Yagi, N. Taketoshi, T. Baba, and Y. Shigesato: *J. Appl. Phys.* **111** (2012) 093701.
- 8) C. Tasaki, N. Oka, T. Yagi, N. Taketoshi, T. Baba, T. Kamiyama, S. Nakamura, and Y. Shigesato: *Jpn. J. Appl. Phys.* **51** (2012) 035802.
- 9) T. Yagi, K. Tamano, Y. Sato, N. Taketoshi, T. Baba, and Y. Shigesato: *J. Vac. Sci. Technol. A* **23** (2005) 1180.
- 10) Y. Xu, R. Kato, and M. Goto: *J. Appl. Phys.* **108** (2010) 104317.
- 11) P. E. Hopkins, P. M. Norris, R. J. Stevens, T. E. Beechem, and S. Graham: *J. Heat Transfer* **130** (2008) 062402.
- 12) P. E. Hopkins, L. M. Phinney, J. R. Serrano, and T. E. Beechem: *Phys. Rev. B* **82** (2010) 085307.
- 13) N. Taketoshi, T. Baba, and A. Ono: *Jpn. J. Appl. Phys.* **38** (1999) L1268.
- 14) N. Taketoshi, T. Baba, and A. Ono: *Meas. Sci. Technol.* **12** (2001) 2064.
- 15) T. Baba, N. Taketoshi, and T. Yagi: *Jpn. J. Appl. Phys.* **50** (2011) 11RA01.
- 16) H. Lyeo and D. G. Cahill: *Phys. Rev. B* **73** (2006) 144301.
- 17) R. M. Costescu, M. A. Wall, and D. G. Cahill: *Phys. Rev. B* **67** (2003) 054302.
- 18) R. J. Stevens, A. N. Smith, and P. M. Norris: *J. Heat Transfer* **127** (2005) 315.
- 19) N. Oka, R. Arisawa, A. Miyamura, Y. Sato, T. Yagi, N. Taketoshi, T. Baba, and Y. Shigesato: *Thin Solid Films* **518** (2010) 3119.
- 20) R. M. Costescu, D. G. Cahill, F. H. Fabreguette, Z. A. Sechrist, and S. M. George: *Science* **303** (2004) 989.
- 21) T. Yagi, N. Taketoshi, and T. Baba: 33rd Japan Symp. Thermophysical Properties, 2012, A114 [in Japanese].
- 22) T. Baba: *Jpn. J. Appl. Phys.* **48** (2009) 05EB04.
- 23) Y. Yamashita, T. Yagi, and T. Baba: *Jpn. J. Appl. Phys.* **50** (2011) 11RH03.
- 24) Japan Society of Thermophysical Properties: *Thermophysical Properties Handbook* (Yokendo, Tokyo, 2008) 2nd ed., p. 25 [in Japanese].